THE JOURNAL OF PHYSICAL CHEMISTRY Letters

Letter

Cite This: J. Phys. Chem. Lett. 2019, 10, 3481−3487

pubs.acs.org/JPCL

Pyrene, a Test Case for Deep-Ultraviolet Molecular Photophysics

Alessandra Picchiotti,[†,§,‡] Artur Nenov,[#,‡] Angelo Giussani,[#,∥,‡] Valentyn I. Prokhorenko,[§] R. J. Dwayne Miller,[*,§,⊥] Shaul Mukamel,[▽] and Marco Garavelli[*,#]

[†]Institute of Physics, ELI Beamlines, Academy of Sciences of the Czech Republic, Na Slovance 2, CZ-18221 Prague, Czech Republic
[§]Max Planck Institute for the Structure and Dynamics of Matter, CFEL (Bld. 99), Luruper Chaussee 149, 22761 Hamburg, Germany
[#]Dipartimento di Chimica Industriale, Università degli Studi di Bologna, Viale del Risorgimento 4, I-40136 Bologna, Italy
[∥]Instituto de Ciencia Molecular, Universitat de València, Apartado 22085, ES-46071 Valencia, Spain
[⊥]Departments of Chemistry and Physics, University of Toronto, Toronto, Ontario M5S 3H6, Canada
[▽]Department of Chemistry, University of California, Irvine, California 92697-2025, United States

Supporting Information

ABSTRACT: We determined the complete relaxation dynamics of pyrene in ethanol from the second bright state, employing experimental and theoretical broadband heterodyne detected transient grating and two-dimensional photon echo (2DPE) spectroscopy, using pulses with duration of 6 fs and covering a spectral range spanning from 250 to 300 nm. Multiple lifetimes are assigned to conical intersections through a cascade of electronic states, eventually leading to a rapid population of the lowest long-living excited state and subsequent slow vibrational cooling. The lineshapes in the 2DPE spectra indicate that the efficiency of the population transfer depends on the kinetic energy deposited into modes required to reach a sloped conical intersection, which mediates the decay to the lowest electronic state. The presented experimental−theoretical protocol paves the way for studies on deep-ultraviolet-absorbing biochromophores ubiquitous in genomic and proteic systems.

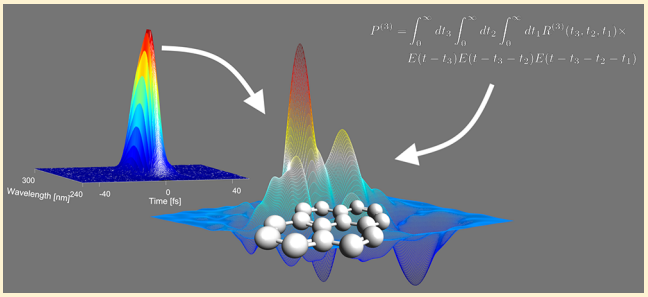

Insight into photoactivated biological functions requires in-depth knowledge of rapid molecular processes. This can be achieved through dynamically resolved spectroscopies that recently became feasible in the deep ultraviolet (UV) below 300 nm.[1−5] Because of enormous challenges in generating broadband laser pulses, two-dimensional photon echo (2DPE) and conventional transient absorption (TA) and transient grating (TG) experiments in the deep-UV are conducted in a one-color fashion with small bandwidth excitation pulses, limiting temporal resolution and informative value, and consequently the informative value of ultrafast processes on the subpicosecond time scale is limited by the temporal resolution.

Studies that combine state-of-the-art electronic structure computations with nonlinear time-resolved spectroscopy techniques and explicitly incorporate excited state absorption (ESA) features from first-principles have successful simulated broadband-probe spectra in the far-IR to near-UV range.[6−13] Simulations of ESA in the deep-UV are challenging because of the high density of states, making imperative the development of a solid theoretical base on simpler molecules.

The objective of this work is pushing the present spectroscopic experimental and theoretical limits. This is done by applying PE, TA, and TG spectroscopy to pyrene, a widely used molecule owing to its interesting photophysical properties[14−20] with such a remarkably long fluorescence and high fluorescence yields. Its well-separated absorption bands with clear Franck−Condon (FC) progressions in the near-UV (lowest bright state at 320 nm) and in the deep-UV (second bright state at 280 nm) make it an excellent model for assessing spectroscopic techniques. The first two-dimensional (2D) electronic broadband spectroscopy in the near UV was performed on pyrene.[21,22]

Technical challenges have limited the study of the de-excitation dynamics from the second bright state. Our experimental and simulation techniques allow for filling the gap. State-of-the-art electronic structure computations (multi-configuration second-order perturbation theory based on restricted active space, RASPT2)[23,24] uncover the deactivation involving ultrafast nonadiabatic transitions mediated by conical intersections (CI). The mechanism is scrutinized by high temporal resolution TA and PE conducted between 240 and 300 nm with ultrashort pulses (6 fs fwhm duration)[25] combined with first-principles spectroscopy simulations.

Figure 1 presents the deep UV linear absorption (LA) experimental and simulated spectra of pyrene in ethanol, resolving the absorption band of the second bright state

Received: May 9, 2019
Accepted: May 13, 2019
Published: May 13, 2019

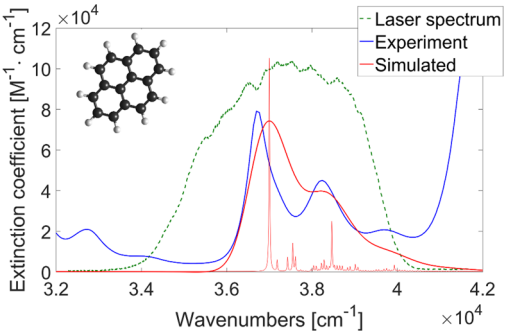

Figure 1. Experimental (blue line) and simulated (red line and stick spectrum) absorption spectra of pyrene, overlapped with the experimental laser spectrum (green dashed line).

labeled $2B_{3u}$ (second state in the B_{3u} irreducible representation of D_{2h} symmetry). A well-resolved vibronic progression with peaks at 272 nm (36.7 kcm^{-1}), 262 nm (38.2 kcm^{-1}), and 252 nm (39.7 kcm^{-1}) is observed.[26] Normal mode analysis reveals that the vibronic structure of the $S_0 \rightarrow 2B_{3u}$ transition is attributable mainly to the 1456 cm^{-1} symmetric carbon−carbon stretching. Low-frequency breathing vibrations at 405 and 592 cm^{-1} are responsible for the shoulder of the 272 nm band. Other symmetric carbon−carbon stretch vibrations form the Raman-active modes (Table 1 and Figure S7), which agree well with earlier Raman data.[26,27] The solvent has little effect on the ES dynamics, as different solvents and environments—ethanol, polycrystalline powder acetonitrile,[26] benzene[27]—provide similar spectra, in agreement with the gas-phase computations. The theoretical 1336 cm^{-1} band is the only missing vibration in the experimental Raman spectra; however, depolarization ratios suggest its existence.[26] The 1242 cm^{-1} band, which is the most intense band in nonresonance Raman, loses intensity in resonance Raman in favor of the 1408 cm^{-1} band, as well as the low-frequency bands at 408 and 592 cm^{-1} with an additional band at 574 cm^{-1} appearing only in resonance Raman. The 1597 cm^{-1} mode, i.e., the characteristic nonfully symmetric vibration of pyrene observed experimentally, is the only intense mode not appearing in the simulation.[26] However, it loses intensity upon exciting the $2B_{3u}$, indicating its smaller importance for dynamics.

The $2B_{3u}$ absorption band is similar to that of the lowest bright state which absorbs around 320 nm, labeled $1B_{2u}$.[26] Resonance Raman spectroscopy of the $1B_{2u}$,[26] as well as previously reported vibrationally resolved LA simulations,[28] reveal that the same high-frequency (1456 cm^{-1}) and low-frequency (405 cm^{-1}) modes are responsible for the $1B_{2u}$ band vibrational progression and broadening.

Figure 2 shows TA spectra up to 200 ps. Because of the extremely strong contribution of the nonlinear solvent response around zero delay and undesirable scattering effects of the solvent in the UV,[29] the early time dynamics cannot be resolved. We observe an intense positive band at 272 nm associated with the bleach of the fundamental, together with two negative ESA signatures at 255 and 265 nm. A weak bleaching at 261 nm matching the first overtone of the $2B_{3u}$ state in the LA spectrum is also present in the experimental TA spectrum, although very faintly because of overlap with the ESA.

Experimentally, the positive signal at 272 nm loses intensity, while the negative band at 255 nm gains in intensity. The decay associated spectra (DAS) were extracted by means of a global analysis, obtaining four lifetimes: 0.75 ps, 8 ps, 24 ps, and an infinitely long lifetime (Figure 3).

The 0.75 ps lifetime is associated with the initial increase of the ESA band intensity, and it is accompanied by the decrease of the positive 272 nm signal, followed by vibrational cooling with an 8 ps lifetime which blue-shifts the maxima of the contributions. The decreasing ESA intensity at later times can be fitted with another exponential curve of 24 ps. The infinitely long lifetime can be representative of either ESA decay or ground-state bleaching (GSB) recovery, a S_1 bottleneck trap, or the sum of multiple phenomena.

The high temporal resolution of our experiments allows the observation of intensity beating in the TA and in the HTG spectra (Figure S20). The Fourier transform of the residuals provides the frequencies responsible for the oscillatory features (Figures S21 and S22; the most intense contributions are provided in Table 1). The extracted frequencies match those from the normal-mode analysis of the $2B_{3u}$ state.[26,27] Because of the overlap of bleach and photoinduced absorption in the probed window, the assignment of the Raman modes is not unambiguous and we do not exclude the possibility of

Table 1. Frequencies (ω, cm^{-1}) and Huang−Rhys (HR) Factors of the Fundamental Raman Modes in Our Simulated Gradient Projection (grad. proj.) Approach and Adiabatic Molecular Dynamics[a]

	simulation				experiment						
	grad. proj.		mol. dynamics		HTG		Raman		res. Raman		
	ω	HR	ω	HR	ω	int	ω	int	ω	int	type
ν_1	405	0.15	425	0.19	390		407	0.33	408	0.40	breathing
ν_2	592	0.26	546/607	0.240/0.157	597	0.28	592	0.26	574/592	0.50	breathing
ν_3					888						
ν_4	1079	0.12	1093	0.06	1073		1066	0.18	1067	0.10	C−C stretch
ν_5	1271	0.10	1275	0.10	1238	0.52	1241	1.00	1242	0.45	C−C stretch
ν_6	1347	0.03	1335	0.07							C−C stretch
ν_7	1456	0.16	1457	0.20	1413	1.00	1406	0.86	1408	1.00	C−C stretch
ν_8	1574	0.06	1578	0.06			1550	0.09	1553	0.10	C−C stretch
ν_9					1592		1594	0.64	1597	0.30	
ν_{10}	1668	0.05	1639	0.03	1626		1628	0.27	1632	0.30	C−C stretch
ν_{11}					2942	0.29					C−H stretch

[a]See section 3.2.1 in the Supporting Information. Frequencies (ω, cm^{-1}) and intensity (int) of the vibrational modes obtained in ethanol by heterodyne transient grating (HTG, this work), from crystalline powder by Raman spectroscopy,[27] and in acetonitrile by resonance Raman.[26]

DOI: 10.1021/acs.jpclett.9b01325
J. Phys. Chem. Lett. 2019, 10, 3481−3487

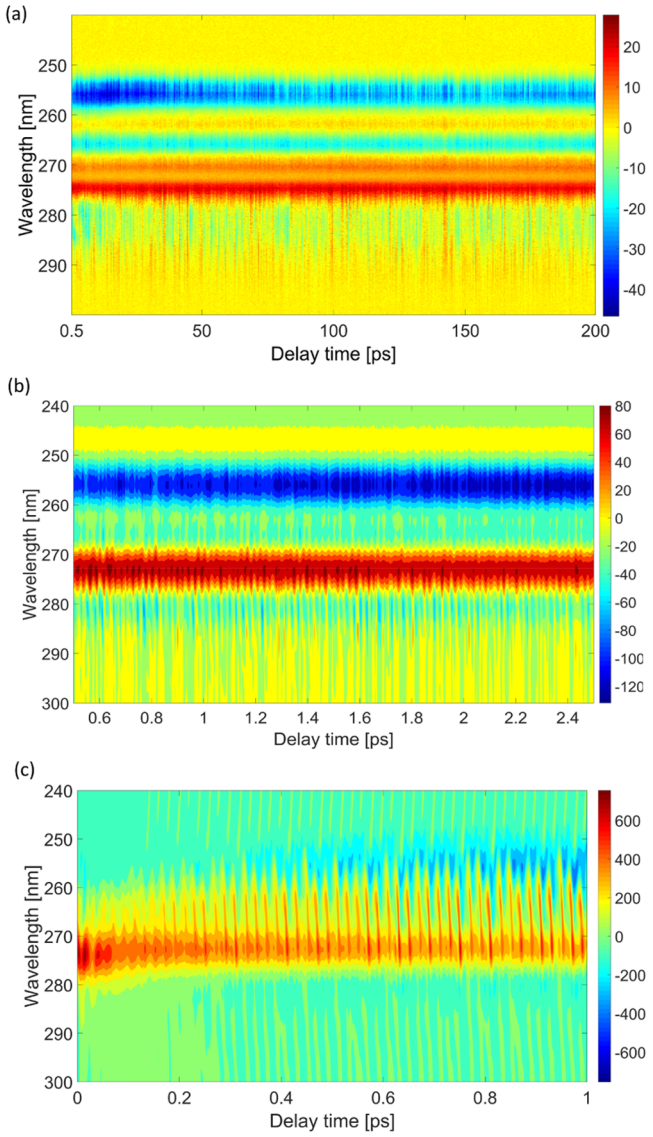

Figure 2. Experimental TA kinetics of pyrene up to 200 ps (a, 500 fs step) and first 2.5 ps of a fine-resolution measurement (b, 20 fs step) measured in ethanol. (c) Simulated TA spectrum up to 1 ps. Colors are in differential transmission dT (counts/a.u.).

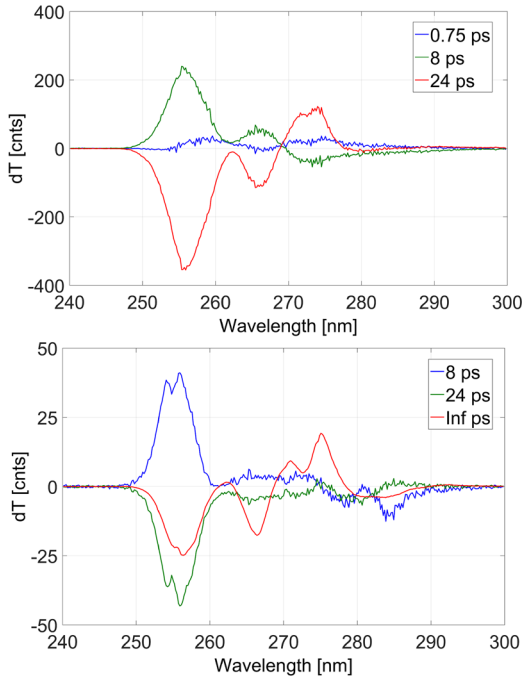

Figure 3. Decay associated spectra from a short time range TA spectrum (top, fitting the TA spectrum from Figure 2b) and a long time range TA spectrum where the longest time constant was fixed to infinity (bottom, fitting the TA spectrum from Figure 2a). Vertical axes are in differential transmission dT (counts/a.u.).

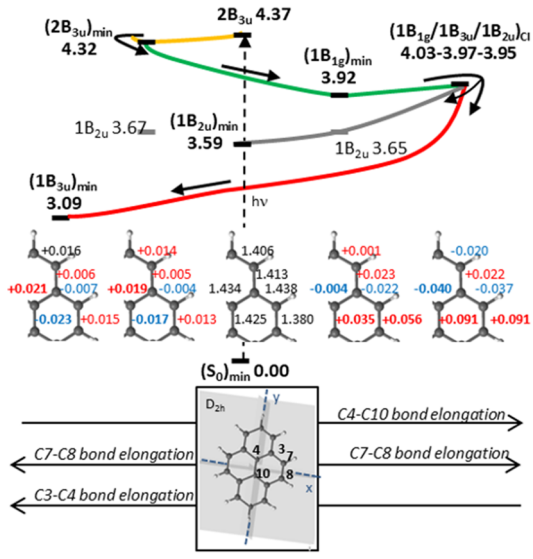

Figure 4. Top: schematic representation of the main decay paths after excitation into the bright $2B_{3u}$ state. Energies are in electronvolts with respect to the ground state. Orange, green, and red indicate the potential energy surfaces of states $2B_{3u}$, $1B_{1g}$, and $1B_{3u}$, respectively. Bottom: characteristic bond lengths (shown in Å) along the nonadiabatic deactivation path to the lowest dark state $1B_{3u}$. Shown are only symmetry-nonequivalent atoms. Inset: mirror planes and rotation axes of pyrene in D_{2h} symmetry.

resolving vibrational coherences in the ground state. However, we note that the 2942 and 888 cm^{-1} modes are absent in Raman experiments, the former being associated only with the 255 nm ESA.

The deactivation mechanism was followed through energy minimization techniques (Figure 4). The FC point exhibits two dark electronic states near the bright $2B_{3u}$ state, denoted as $1B_{1g}$ and $2B_{1g}$ (Table S4). The near degeneracy allows ultrafast nonadiabatic population transfer to $1B_{1g}$. Because of missing stimulated emission (SE) signatures in the TA spectrum, we assume that $2B_{3u}$ decays to $1B_{1g}$ before probing is initiated (i.e., before 200 fs). This assumption has been recently confirmed experimentally in a two-color (deep-UV pump visible-probe) TA experiment.[22]

According to our computations, the lowest bright state $1B_{2u}$ is not involved in the immediate relaxation after $2B_{3u}$ excitation. A nearly constant 0.5 eV $2B_{3u}/1B_{2u}$ gap is observed in both static and dynamic calculations on the $2B_{3u}$ state, rationalized by the identical vibrational modes (1456 and 405 cm^{-1}) characterizing both states (sec. 3.2.3 of the Supporting Information).

The $1B_{1g}$ state exhibits a considerable energetic stabilization with a minimum 0.4 eV below the $2B_{3u}$ minimum. Molecular orbital analysis at the $1B_{1g}$ minimum demonstrates that geometrical deformations leading toward a CI with the state

DOI: 10.1021/acs.jpclett.9b01325
J. Phys. Chem. Lett. 2019, 10, 3481−3487

$1B_{2u}$ destabilize more substantially the dark state $1B_{3u}$, so that CI optimization encounters a three-state CI($1B_{1g}/1B_{3u}/1B_{2u}$) about 0.08 eV above the $1B_{1g}$ minimum. D_{2h} symmetry is reduced at the CI to C_{2v}. This is realized along with a 350 cm^{-1} in-plane bending mode of $1B_{2u}$ symmetry, which creates a coupling between the $1B_{1g}$ and $1B_{3u}$ states. In fact, while the gradient difference vector at the CI is of A_g symmetry (having large overlap with the 1668 cm^{-1} mode), the derivative coupling vector exhibits a large overlap with the 350 cm^{-1} mode of $1B_{2u}$ symmetry. These observations indicate that at the three-state CI the wave packet populates the $1B_{3u}$ state. The nonadiabatic transfer is facilitated by the same set of 12 modes of B_{2u} symmetry, enabling the $2B_{3u} \rightarrow 1B_{1g}$ decay. We assign the 0.75 ps lifetime to the decay through the CI. The relatively long excited-state lifetime with respect to the sub-100 fs lifetimes of the bright states $1B_{2u}$ and $2B_{3u}$[30,31] could be rationalized by the time required to distribute energy in the decay-determining 1668 cm^{-1} mode, which has a small Huang–Rhys factor of 0.05 in the $2B_{3u}$ state, as required in order to overcome the 0.1 eV barrier to reach the CI. Static fluorescence spectra collected after 260 nm excitation (Figure 5) show a small shoulder between 350 and 368 nm associated with $1B_{2u}$ emission.[32] Nevertheless, the short lifetime of the $1B_{2u}$ state strongly suggests that no significant population could accumulate that could be the source of a measurable spectroscopic signal from $1B_{2u}$.[30,31]

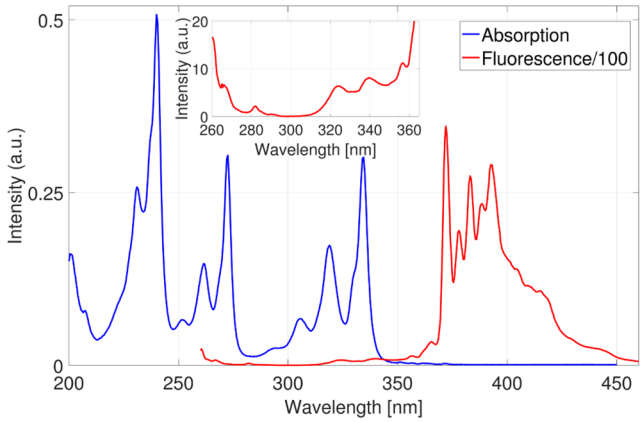

Figure 5. Static fluorescence emission spectrum of pyrene in ethanol. Excitation wavelength, 260 nm; excitation slid, 20 mm; emission slid, 1.5 mm. Average time of acquisition for each wavelength is 5 s.

Upon transfer to the $1B_{3u}$ state, pyrene encounters a steep potential toward equilibrium. A weak feature between 300 and 350 nm in the static fluorescence spectrum is tentatively assigned to the vibrational dynamics in the hot $1B_{3u}$ state. According to simulations, half of the potential energy is stored in two modes: the 350 cm^{-1} in-plane bending (B_{2u} symmetry) and a 1668 cm^{-1} carbon–carbon stretching (A_g symmetry, Figure S8). In support of our mechanism, we draw the reader's attention to a recently reported two-color (deep-UV pump visible-probe) TA experiment by Borrego-Varillas et al. Therein, the authors report a quantum beat with a frequency of 390 cm^{-1} shown unambiguously to arise from the wavepacket on S_1 after pumping the $2B_{3u}$ state at 270 nm.[22] The quantum beat can be attributed to dynamics along a symmetric mode (a 410 cm^{-1} mode has been observed in Raman experiments, see Table 1), which unexpectedly gains in intensity after decay to S_1 in contrast to other Raman modes (e.g., 590 cm^{-1}, not observed by Borrego-Varillas et al.). We note however that the frequency of 390 cm^{-1} matches closely that of the 350 cm^{-1} in-plane bending mode, predicted by our calculations to dominate the vibrational dynamics on the S_1 state after passage through the three-state CI. The temporal resolution of the experiment of Borrego-Varillas et al. (~16 fs) does not allow the detection of the other dominant mode (1668 cm^{-1}) predicted by our model. Studies on azobenzene and rhodopsin have shown that large amounts of energy into a few modes could induce intensity beats in the TA lasting for picoseconds.[8,12] Thus, the 8 and 24 ps lifetimes can be associated with vibrational cooling of photoactive vibrational modes.

Following the proposed mechanism, we simulated the TA spectrum up to 1 ps. After the pump pulse, we observe SE out of $2B_{3u}$, which enhances the signal intensity in the GSB region (270–275 nm) and reaches down to 290 nm. The $2B_{3u}$ state shows a weak ESA band around 250–260 nm which partially cancels the second vibronic band at 262 nm. Our calculations predict further characteristic fingerprints around 360 and 540 nm, observed recently experimentally.[22] The $2B_{3u}$ fingerprint

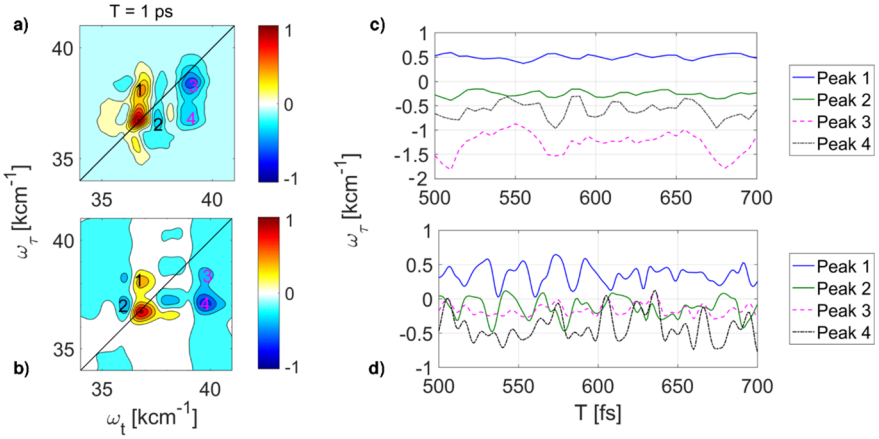

Figure 6. Experimental (a) and simulated (b) 2D maps of pyrene at waiting time of 1000 fs. Experimental (c) and simulated (d) intensity fluctuations of selected peaks in the 2DPE. Photoinduced absorption signal PA1, which gives rise to peak 2 in panel a appears red-shifted below the diagonal bleach signal in the simulated spectrum (b). A Fourier transform of the oscillations in panel c is shown in the Supporting Information (Figure S27).

DOI: 10.1021/acs.jpclett.9b01325
J. Phys. Chem. Lett. 2019, 10, 3481–3487

signals decay on a 100 fs time scale. (A phenomenological 100 fs lifetime was adopted for the $2B_{3u} \rightarrow 1B_{1g}$ population transfer in agreement with recent findings by Borrego-Varillas et al.[22]) At later times new signatures appear: a strong ESA between 250 and 260 nm (labeled PA_1) and a weaker ESA around 280 nm (labeled PA_2). Both peaks are fingerprints of the $1B_{3u}$ state populated with the 0.75 ps lifetime. The $1B_{3u}$ state exhibits further characteristic ESA in the near-UV at 370 nm and in the visible at 475 nm,[9,21,22] potentially accessible through a two-color pump−probe setup. PA_2 overlaps strongly with the GSB and is responsible for the intensity beat pattern in the 270 nm region. Simulated TA shows intensity beating due to the vibrational dynamics in the pair of $1B_{3u}$-specific modes 350 and 1668 cm^{-1}. The experimental TA also shows an intensity beat pattern, with weak contributions from the pair of $1B_{3u}$-specific modes. However, the 1413, 1238, and 597 cm^{-1} modes dominate the modulation of the ESA signatures, previously assigned to the $2B_{3u}$ state. A progression of 1450 cm^{-1} is visible at 300−350 nm in the static fluorescence spectrum, indicating memory conservation upon departure from the $2B_{3u}$ state, a mechanism not implemented in our simulations, leading to overemphasizing $1B_{3u}$-specific modes. The $1B_{1g}$ state intermediately populated in the relaxation has no characteristic ESA in the probed spectral window, but our calculations show that it exhibits absorption features in the visible which could be addressed to scrutinize the proposed model. Two close-lying states absorbing 3.6−3.8 eV above the S_3 equilibrium would lead to an intense signal in the transient spectra around 330 nm. Thus, we propose a two-color, deep-UV pump near-UV probe, experiment with pulses centered at 290 and 330 nm, respectively, for validating the $1B_{1g}$ involvement.

Figure 6 shows experimental and simulated 2DPE spectra at a 1000 fs waiting time. Spectra at further waiting times are provided in section 4.1 (simulation) and section 11 (experiment) of the Supporting Information. A checkerboard pattern of positive and negative contributions along two stripes at ω_τ = 36.7 kcm^{-1} and ω_τ = 38.2 kcm^{-1} corresponding respectively to the fundamental and the first overtone of the $2B_{3u}$ band is shown. Diagonal bleach contributions (positive, red color) are detected at (36.7, 36.6) kcm^{-1} and (38.0, 38.2) kcm^{-1} in the experiment, while off-diagonal bleach contributions are encountered at (38.0, 36.7) kcm^{-1} (intense, above diagonal) and at (37.0, 38.2) kcm^{-1} (weak, below diagonal). The pattern arises from strong coupling of the electronic transition to the high-frequency carbon−carbon stretching. The signals are characterized by an oscillatory intensity. Theoretical simulations reproduce the experimental bleach pattern and its dynamics, allowing for the separation of individual contributions to the PE. The intensity oscillations (period of approximately 22 fs) are associated with the dynamics of an interstate coherence created by the pump−pulse pair between the fundamental and first overtone in the potential of the carbon−carbon stretch. At early times (first 100 fs), for which only simulations are available, the spectra resolve additional peaks below 36.0 kcm^{-1} resulting from the strong SE out of the $2B_{3u}$ state (sec. 4.2 in the Supporting Information). Their absence in the experimental PE spectra supports that $2B_{3u}$ decays on a sub-200 fs time scale. There are several $2B_{3u}$ fingerprints contributing to the ESA at early times, but their transition dipole moments are orthogonal to the dipole moment of the GS-$2B_{3u}$ transition, consequently appearing weak when all pulses have identical polarizations (Figure S11). Instead, a cross-polarized pump−probe pair of pulses would enhance the intensity ESA signatures (Figure S12).

The bleach pattern is typical for vibrational coherences in a coupled two-level system.[33] Further negative contributions appear in the PE spectrum at approximately ω_t = 36.0 kcm^{-1}, ω_t = 37.5 kcm^{-1}, and ω_t = 39 kcm^{-1}, associated with the mentioned ESA signatures PA1 and PA2 observed also in the TA spectrum. PA_1 spreads from ω_t = 35.5 to ω_t = 37.5 kcm^{-1} and falls under the bleach of the fundamental. PA_2 exhibits a vibrational progression from ω_t = 37.0 kcm^{-1} to ω_t = 40.0 kcm^{-1} with absorptive and dispersive features associated with the dynamics in the 1660 cm^{-1} mode connecting the CI with the $1B_{3u}$ minimum. It covers completely the bleach of the second overtone. Both PA_1 and PA_2 lead to the ESA feature at ω_t = 37.5 kcm^{-1} which interferes with the bleach of the first overtone (see sec. 4.3 in the Supporting Information). The bleach−ESA interference, although complicating the analysis of the spectral dynamics, is essential for interpreting the spectra.

The experimental 2D spectrum shows a very intense ESA contribution along the trace of the overtone at (ω_τ, ω_t) = (38.2 kcm^{-1}, 39.0 kcm^{-1}) in disagreement with theory. This feature is observable only with broad-band UV-ES 2D spectroscopy. Tentatively, this pronounced ESA intensity could be assigned to the weak bleach contribution at the "overtone" pump frequency (whereas it is stronger at the "fundamental" pump frequency, canceling the ESA more effectively). This interpretation does not hold for long delay times when the system has relaxed in the lowest S_1 vibrational level and the probe signal is no longer correlated with the pump frequency. Consequently, at longer delay times, the signal at a certain probe frequency ω_t should be understood as a convolution of the electronic probe spectrum of the lowest vibrational level with the pump (i.e., linear absorption) spectrum. The most intense band in the LA spectrum is that of the "fundamental" frequency and so should be signals along the "fundamental" pump frequency in the 2DES spectrum at longer delay times. However, the intense ESA along the "overtone" pump frequency survives for tens of ps. A more plausible interpretation of this long-lasting feature is that the population transfer to $1B_{3u}$ is more efficient when the overtone of the $2B_{3u}$ band is excited, because of additional kinetic energy in the carbon−carbon stretch at disposal for reaching the sloped CI($1B_{1g}$/$1B_{3u}$/$1B_{2u}$), whereas part of the population excited in the fundamental remains trapped in the $1B_{1g}$ state.

A combination of experimental and theoretical advances has been applied for the first time to record and interpret the pyrene time-resolved broadband spectroscopy in the deep-UV (250−300 nm). On the basis of TA, HTG, and 2D PE experiments and state-of-the-art electronic-structure computations, we propose a model for the deactivation following excitation of the second bright $2B_{3u}$ state. Computations reveal an ultrafast sub-200 fs depopulation of the bright state into a dark state $1B_{1g}$, which has neither emissive nor absorptive features in the probed spectral region. The emergence of a prominent ESA band at 250 nm in the TA and HTG spectra with a build-up time of 0.75 ps is shown to match the population time of the lowest dark state $1B_{3u}$ that acts as a bottleneck and is accessed via a sloped three-state conical intersection. The process exhibits characteristic ESA signatures, reproduced in the simulations.

While the first bright $1B_{2u}$ state decays within ∼100 fs,[30,31] the second bright state $2B_{3u}$ lives 1 order of magnitude longer

DOI: 10.1021/acs.jpclett.9b01325
J. Phys. Chem. Lett. 2019, 10, 3481−3487

in the higher-lying ES manifold. Long-lasting intensity oscillations with a dampening time of tens of picoseconds indicate weak coupling with the environment, in agreement with the picosecond-lasting lifetimes, and associated with vibrational cooling on the lowest trapping $1B_{3u}$ state.

The unprecedented high temporal resolution of our setup allowed for the identification of high-frequency carbon−carbon stretch vibrations as the modes responsible for the vibrational progression in the LA, the intensity beats in the TA, and the checkerboard pattern of the 2DPE spectra. Bleach−ESA signal interference leads to coherent oscillations with a complex pattern, making simulations essential to disentangle individual contributions. A prominent feature present in the 2DPE spectra is an intense ESA contribution along the trace of the $2B_{3u}$ overtone. This suggests that the efficiency of the population transfer to the $1B_{3u}$ state is enhanced when more kinetic energy is deposited into the driving modes in agreement with the sloped nature of the conical intersection found along the decay path.

Experiments to further scrutinize the proposed mechanism have been proposed. The joint experimental−theoretical protocol developed and applied here sets the stage for similar studies on the deep-UV-absorbing biorelevant chromophores found in DNA and proteins.

■ ASSOCIATED CONTENT

Supporting Information

The Supporting Information is available free of charge on the ACS Publications website at DOI: 10.1021/acs.jpclett.9b01325.

Sample preparation, experimental setup, data analysis, more experimental and simulated results, simulation protocols for nonlinear spectroscopy and molecular dynamics, simulation parameters, simulated spectra, molecular orbitals, and Cartesian coordinates (PDF)

■ AUTHOR INFORMATION

Corresponding Authors

*E-mail: marco.garavelli@unibo.it.
*E-mail: dmiller@lphys2.chem.utoronto.ca.

ORCID

Alessandra Picchiotti: 0000-0003-0167-1431
Artur Nenov: 0000-0003-3071-5341
Angelo Giussani: 0000-0002-9452-7641
R. J. Dwayne Miller: 0000-0003-0884-0541
Shaul Mukamel: 0000-0002-6015-3135
Marco Garavelli: 0000-0002-0796-289X

Author Contributions

‡A.P., A.N., and A.G. contributed equally.

Notes

The authors declare no competing financial interest.

■ ACKNOWLEDGMENTS

The fluorescence spectrum was taken in the laboratory of Prof. Dr. Henning Tidow (Universitaet Hamburg). This work was supported by the European Research Council Advanced Grant STRATUS (ERC-2011-AdG No. 291198).

■ REFERENCES

(1) Baum, P.; Lochbrunner, S.; Riedle, E. Generation of tunable 7-fs ultraviolet pulses: achromatic phase matching and chirp management. *Appl. Phys. B: Lasers Opt.* **2004**, *79*, 1027−1032.
(2) Cowan, M. L.; Bruner, B. D.; Huse, N.; Dwyer, J. R.; Chugh, B.; Nibbering, E. T. J.; Elsaesser, T.; Miller, R. J. D. Ultrafast memory loss and energy redistribution in the hydrogen bond network of liquid H_2O. *Nature* **2005**, *434*, 199−202.
(3) Selig, U.; Schleussner, C.-F.; Foerster, M.; Langhojer, F.; Nuernberger, P.; Brixner, T. Coherent two-dimensional ultraviolet spectroscopy in fully noncollinear geometry. *Opt. Lett.* **2010**, *35*, 4178−4180.
(4) Cannizzo, A. Ultrafast UV spectroscopy: from a local to a global view of dynamical processes in macromolecules. *Phys. Chem. Chem. Phys.* **2012**, *14*, 11205−11223.
(5) Chergui, M. Ultrafast molecular photophysics in the deep-ultraviolet. *J. Chem. Phys.* **2019**, *150*, 070901.
(6) Prokhorenko, V. I.; Picchiotti, A.; Pola, M.; Dijkstra, A. G.; Miller, R. J. D. New Insights into the Photophysics of DNA Nucleobases. *J. Phys. Chem. Lett.* **2016**, *7* (22), 4445−4450.
(7) Segarra-Martí, J.; Mukamel, S.; Garavelli, M.; Nenov, A.; Rivalta, I. Towards Accurate Simulation of Two-Dimensional Electronic Spectroscopy. *Top. Curr. Chem.* **2018**, *376*, 24.
(8) Nenov, A.; Borrego-Varillas, R.; Oriana, A.; Ganzer, L.; Segatta, F.; Conti, I.; Segarra-Marti, J.; Omachi, J.; Dapor, M.; Taioli, S.; et al. UV-Light-Induced Vibrational Coherences: The Key to Understand Kasha Rule Violation in trans-Azobenzene. *J. Phys. Chem. Lett.* **2018**, *9*, 1534−1541.
(9) Nenov, A.; Giussani, A.; Fingerhut, B. P.; Rivalta, I.; Dumont, E.; Mukamel, S.; Garavelli, M. Spectral lineshapes in nonlinear electronic spectroscopy. *Phys. Chem. Chem. Phys.* **2015**, *17*, 30925−30936.
(10) Borrego-Varillas, R.; Teles-Ferreira, D. C.; Nenov, A.; Conti, I.; Ganzer, L.; Manzoni, C.; Garavelli, M.; De Paula, A. M.; Cerullo, G. Observation of the sub-100 fs population of a dark state in a thiobase mediating intersystem crossing. *J. Am. Chem. Soc.* **2018**, *140*, 16087−16093.
(11) Johnson, P. J.; Farag, M. H.; Halpin, A.; Morizumi, T.; Prokhorenko, V. I.; Knoester, J.; Jansen, T. L.; Ernst, O. P.; Miller, R. D. The Primary Photochemistry of Vision Occurs at the Molecular Speed Limit. *J. Phys. Chem. B* **2017**, *121*, 4040−4047.
(12) Farag, M. H.; Jansen, T. L. C.; Knoester, J. The origin of absorptive features in the two-dimensional electronic spectra of rhodopsin. *Phys. Chem. Chem. Phys.* **2018**, *20*, 12746−12754.
(13) Roos, M. K.; Reiter, S.; de Vivie-Riedle, R. Ultrafast relaxation from 1La to 1Lb in pyrene: a theoretical study. *Chem. Phys.* **2018**, *515*, 586−595.
(14) Reichardt, C. Solvatochromic Dyes as Solvent Polarity Indicators. *Chem. Rev.* **1994**, *94*, 2319−2358.
(15) Winnik, F. M. Photophysics of preassociated pyrenes in aqueous polymer solutions and in other organized media. *Chem. Rev.* **1993**, *93*, 587−614.
(16) França, B. M. de; Bello Forero, J. S.; Garden, S. J.; Ribeiro, E. S.; Souza, R. da S.; Teixeira, R. S.; Corrêa, R. J. Green fluorescence pyrene-based dye as a new p-extended system: Synthesis, photophysical and theoretical studies. *Dyes Pigm.* **2018**, *148*, 444−451.
(17) Kwon, J.; Park, S. K.; Lee, Y.; Lee, J. S.; Kim, J. Tailoring chemically converted graphenes using a water-soluble pyrene derivative with a zwitterionic arm for sensitive electrochemiluminescence-based analyses. *Biosens. Bioelectron.* **2017**, *87*, 89−95.
(18) Ruzicka, P.; Kral, T. *Pyrene: Chemical Properties, Biochemistry Applications and Toxic Effects*; Chemistry Research and Applications Series; Nova Publishers, 2013.
(19) Figueira-Duarte, T. M.; Müllen, K. Pyrene-based materials for organic electronics. *Chem. Rev.* **2011**, *111*, 7260−7314.
(20) Niko, Y.; Didier, P.; Mely, Y.; Konishi, G.; Klymchenko, A. S. Bright and photostable push-pull pyrene dye visualizes lipid order variation between plasma and intracellular membranes. *Sci. Rep.* **2016**, *6*, 18870.

DOI: 10.1021/acs.jpclett.9b01325
J. Phys. Chem. Lett. 2019, 10, 3481−3487

(21) Krebs, N.; Pugliesi, I.; Hauer, J.; Riedle, E. Two-dimensional Fourier transform spectroscopy in the ultraviolet with sub-20 fs pump pulses and 250−720 nm supercontinuum probe. *New J. Phys.* **2013**, *15*, 085016.
(22) Borrego-Varillas, R.; Ganzer, L.; Cerullo, G.; Manzoni, C. Ultraviolet Transient Absorption Spectrometer with Sub-20-fs Time Resolution. *Appl. Sci.* **2018**, *8*, 989.
(23) Malmqvist, P.-Å.; Rendell, A.; Roos, B. O. The restricted active space self-consistent-field method, implemented with a split graph unitary group approach. *J. Phys. Chem.* **1990**, *94*, 5477−5482.
(24) Malmqvist, P.-Å.; Pierloot, K.; Shahi, A. R. M.; Cramer, C. J.; Gagliardi, L. The restricted active space followed by second-order perturbation theory method: theory and application to the study of CuO_2 and Cu_2O_2 systems. *J. Chem. Phys.* **2008**, *128*, 204109.
(25) Prokhorenko, V. I.; Picchiotti, A.; Maneshi, S.; Miller, R. J. D. Broadband Electronic Two-Dimensional Spectroscopy in the Deep UV. In *Springer Proceedings in Physics*; Yamanouchi, K., Cundiff, S., de Vivie-Riedle, R., Kuwata-Gonokami, M., DiMauro, L., Eds.; Springer International Publishing, 2015; Vol. *162*, p 432.
(26) Jones, C. M.; Asher, S. A. Ultraviolet Resonance Raman Study of the Pyrene S_4, S_3, and S_2 Excited Electronic States. *J. Chem. Phys.* **1988**, *89*, 2649.
(27) Shinohara, H.; Yamakita, Y.; Ohno, K. Raman spectra of polycyclic aromatic hydrocarbons. Comparison of calculated Raman intensity distributions with observed spectra for naphthalene, anthracene, pyrene, and perylene. *J. Mol. Struct.* **1998**, *442*, 221−234.
(28) Freidzon, A. Y.; Valiev, R. R.; Berezhnoy, A. A. Ab initio simulation of pyrene spectra in water matrices. *RSC Adv.* **2014**, *4*, 42054−42065.
(29) West, B. a.; Molesky, B. P.; Giokas, P. G.; Moran, A. M. Uncovering molecular relaxation processes with nonlinear spectroscopies in the deep UV. *Chem. Phys.* **2013**, *423*, 92−104.
(30) Neuwahl, F. V. R.; Foggi, P. Direct observation of S2-S1 internal conversion in pyrene by femtosecond transient absorption. *Laser Chem.* **1999**, *19*, 375−379.
(31) Foggi, P.; Pettini, L.; Santa, I.; Righini, R.; Califano, S. Transient absorption and vibrational relaxation dynamics of the lowest excited singlet state of pyrene in solution. *J. Phys. Chem.* **1995**, *99*, 7439−7445.
(32) Baba, H.; Aoi, M. Vapor-phase fluorescence spectra from the second excited singlet state of pyrene and its derivatives. *J. Mol. Spectrosc.* **1973**, *46*, 214−222.
(33) Butkus, V.; Valkunas, L.; Abramavicius, D. Molecular vibrations-induced quantum beats in two-dimensional electronic spectroscopy. *J. Chem. Phys.* **2012**, *137*, 044513.

DOI: 10.1021/acs.jpclett.9b01325
J. Phys. Chem. Lett. 2019, 10, 3481−3487